



HAL
open science

Shallow marine ecosystem collapse and recovery during the Paleocene-Eocene Thermal Maximum

Skye Yunshu Tian, Moriaki Yasuhara, Huai-Hsuan Huang, Fabien L.
Condamine, Marci Robinson

► **To cite this version:**

Skye Yunshu Tian, Moriaki Yasuhara, Huai-Hsuan Huang, Fabien L. Condamine, Marci Robinson. Shallow marine ecosystem collapse and recovery during the Paleocene-Eocene Thermal Maximum. *Global and Planetary Change*, 2021, 207, pp.103649. 10.1016/j.gloplacha.2021.103649 . hal-03383039

HAL Id: hal-03383039

<https://hal.science/hal-03383039>

Submitted on 18 Oct 2021

HAL is a multi-disciplinary open access archive for the deposit and dissemination of scientific research documents, whether they are published or not. The documents may come from teaching and research institutions in France or abroad, or from public or private research centers.

L'archive ouverte pluridisciplinaire **HAL**, est destinée au dépôt et à la diffusion de documents scientifiques de niveau recherche, publiés ou non, émanant des établissements d'enseignement et de recherche français ou étrangers, des laboratoires publics ou privés.

1 **Shallow marine ecosystem collapse and recovery during the Paleocene-Eocene**
2 **Thermal Maximum**

3

4 Skye Yunshu Tian,^{a,1,2} Moriaki Yasuhara,^{a,1,2} Huai-Hsuan M. Huang^{a,b,1}, Fabien L.
5 Condamine^{c,1}, Marci M. Robinson^{d,1}

6

7 ^a School of Biological Sciences, Division for Ecology & Biodiversity, Swire Institute
8 of Marine Science, and State Key Laboratory of Marine Pollution, the University of
9 Hong Kong, Kadoorie Biological Sciences Building, Pokfulam Road, Hong Kong
10 SAR, China.

11 ^b Department of Paleobiology, National Museum of Natural History, Smithsonian
12 Institution, Washington DC 20013-7012.

13 ^c Institut des Sciences de l'Evolution de Montpellier, CNRS, IRD, EPHE, Université
14 de Montpellier, Montpellier, France.

15 ^d Florence Bascom Geoscience Center, U.S. Geological Survey, Reston, Virginia,
16 USA.

17 ¹All authors contributed equally to this work.

18 ²To whom correspondence should be addressed.

19 Emails: u3514102@connect.hku.hk; moriakiyasuhara@gmail.com;

20 Tel: (852) 68438415; (852) 22990317

21 Fax: (852) 25599114

22 **Key words:** Extinction; Ostracoda; Sea level; Warming; Deoxygenation; Habitat
23 compression; PETM; Salisbury Embayment

24 **Abstract**

25 The Paleocene-Eocene Thermal Maximum (PETM), the most well-studied transient
26 hyperthermal event in Earth history, is characterized by prominent and dynamic
27 changes in global marine ecosystems. Understanding such biotic responses provides
28 valuable insights into future scenarios in the face of anthropogenic warming. However,
29 evidence of the PETM biotic responses is largely biased towards deep-sea records,
30 whereas shallow-marine evidence remains scarce and elusive. Here we investigate a
31 shallow-marine microfaunal record from Maryland, eastern United States, to
32 comprehensively document the shallow-marine biotic response to the PETM. We
33 applied birth-death modeling to estimate the local diversity dynamics, combined with
34 evaluation of time-variable preservation artifacts. We discovered strong increase of
35 species disappearance and appearance predating the onset and at the final recovery
36 phase of the PETM, respectively. Our paleoecological analyses indicate that
37 bathymetric habitat compression due to extreme warmth and oxygen minimum zone
38 expansion caused shallow-marine benthic species extirpation and ecosystem
39 perturbation during the PETM; and that rapid recovery and diversification followed
40 the PETM disaster, thus contributing new understanding to the shallow-marine biotic
41 changes in a broad context of global warming.

42

43

44

45

46

47 **Introduction**

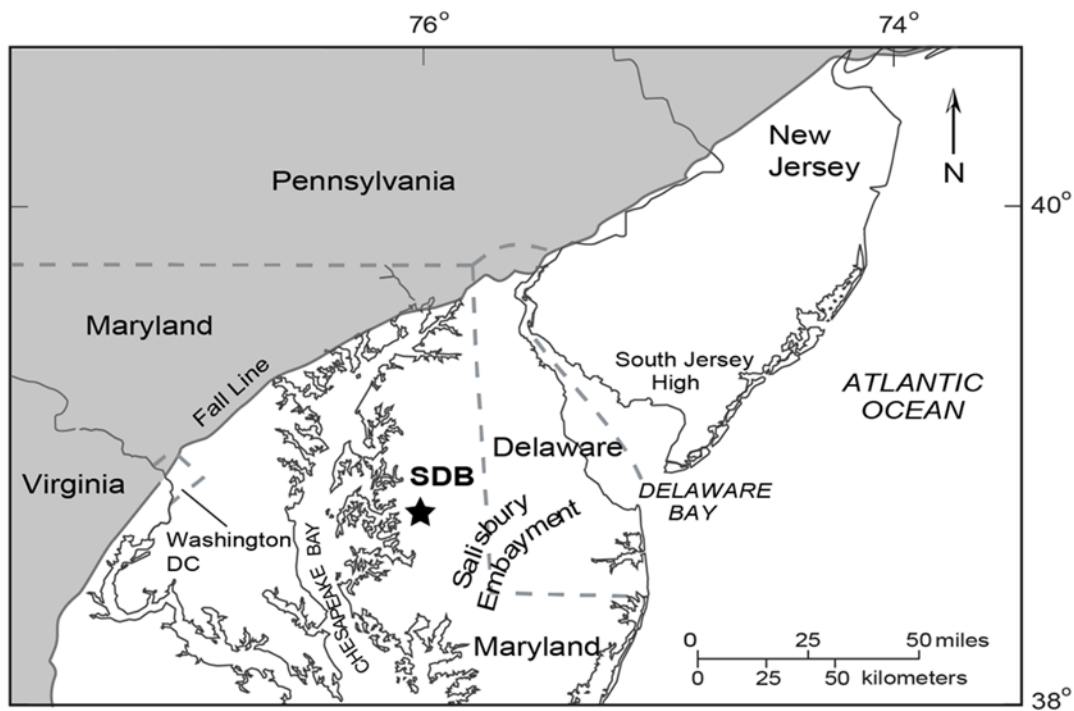
48 The Paleocene-Eocene Thermal Maximum (PETM; ~56 Ma), characterized by
49 a negative carbon isotope excursion (CIE) in both marine and continental sedimentary
50 records, is an abrupt (onset <5 ka (Foster et al., 2018; Turner et al., 2017)) climatic
51 event of extreme global warmth superimposed on long-term greenhouse climate
52 conditions (McInerney and Wing, 2011; Sluijs et al., 2007a). How Earth's biota
53 responded to the PETM has been a prime research question, as the PETM could be the
54 best natural analog to the ongoing and future anthropogenic warming and resulting
55 ecosystem perturbation.

56 The impacts of the PETM climate anomaly on the pelagic ecosystems seem to
57 be relatively mild in general as most groups underwent prominent but transient
58 changes (Speijer et al., 2012). While calcareous nannoplankton show substantial
59 extinction (Speijer et al., 2012), planktic foraminifera, dinoflagellates, and
60 radiolarians show poleward range shifts (McInerney and Wing, 2011; Speijer et al.,
61 2012). Planktic foraminifera also exhibit rapid evolution of distinctive and short-lived
62 “excursion species” that persisted only during the PETM (Kelly et al., 1996). Deep-
63 sea (bathyal-abyssal) benthic ecosystems were severely perturbed during the PETM as
64 the biotic responses are characterized by strong and rapid benthic foraminiferal
65 extinction marking the end of the “Cretaceous” deep-sea fauna, strong faunal turnover,
66 and the resulting establishment of post-Paleocene faunas (Arreguin-Rodriguez et al.,
67 2018; Kennett and Stott, 1991; McInerney and Wing, 2011; Thomas, 2007). In
68 contrast to the well-studied deep-sea PETM records, relatively less attention has been
69 paid to the shallow-marine (neritic) benthic ecosystems, with varying biotic responses
70 documented yet a synthetic understanding lacking (Self-Trail et al., 2017; Speijer et
71 al., 2012). Shallow-marine mollusks do not show substantial differences between pre-

72 and post-PETM faunas, suggesting an almost imperceptible long-term impact of the
73 PETM (Foster et al., 2020; Ivany et al., 2018). Coral reefs declined at the end of the
74 Paleocene, and larger benthic foraminifera took over the position of dominant
75 carbonate producers in the early Eocene (Kiessling and Simpson, 2011; Scheibner and
76 Speijer, 2008; Speijer et al., 2012). However, the shallow-marine microfossil record
77 ‘sandwiches’ the PETM without data from the PETM core, because of either poor
78 microfossil occurrence or preservation, thus lacking documentation of potential
79 transient changes (Foster et al., 2020; Ivany et al., 2018). Therefore shallow-marine
80 benthic PETM records are generally limited to microfossils. Shallow-marine benthic
81 foraminiferal assemblages show changes in species composition and a transient
82 decline in diversity rather than extinction at the PETM (Speijer et al., 2012; Stassen et
83 al., 2015).

84 Ostracods (seed shrimps: Arthropoda) are the only benthic microfossil other
85 than benthic foraminifera and the only marine metazoan invertebrate that leaves fossil
86 records rich enough to reconstruct a detailed biotic response to the PETM of high
87 temporal resolution. Ostracods are therefore considered the surrogate of other
88 metazoan invertebrates in respect to benthic biotic response (Yasuhara and Cronin,
89 2008; Yasuhara et al., 2008). Documented deep-sea ostracod responses to the PETM
90 include 1) taxonomic loss of variable magnitude (from 64 to 25% diversity decrease)
91 due to local extinction and/or species geographic range shifts, 2) community
92 restructuring with high dominance of opportunistic and/or generalist taxa, 3) dwarfing,
93 and 4) shell morphological changes (Lewis Steineck and Thomas, 1996; Webb et al.,
94 2009; Yamaguchi and Norris, 2012; Yamaguchi and Norris, 2015; Yamaguchi et al.,
95 2012). A few studies have investigated PETM shallow-marine ostracods and found
96 strong faunal turnovers (Morsi et al., 2011; Speijer et al., 2012; Speijer and Morsi,

97 2002), but further synthesis of the general patterns of shallow-marine benthic biotic
98 response has been hampered by various uncertainties including the existence of
99 unconformities between depositional units, varying fossil preservation states, and low



100 fossil abundance.

101 **Fig. 1.** Map showing the location of the South Dover Bridge (SDB) core in the
102 Salisbury Embayment, southeastern Maryland, USA.

103

104 In this study, we investigated the ostracod assemblage from a near-complete
105 PETM section from the Salisbury Embayment of the mid-Atlantic Coastal Plain (Fig.
106 1). In the Atlantic Coastal Plain, the PETM sections deposited in inner to outer neritic
107 environments are highly expanded due to high sedimentation rates and can be nearly
108 complete (John et al., 2008; León y León et al., 2018; Self-Trail et al., 2017). We
109 employed recently developed process-based birth-death modeling to handle time-

110 variable and taxon-specific preservation issues, to properly document the shallow-
111 marine benthic biotic changes in relation to warming, dissolved oxygen decline and
112 other characteristic ecological stressors of the PETM that might be partially analogous
113 to those of ongoing anthropogenic warming (Zachos et al., 2008). For example,
114 bathymetric habitat compression may be occurring in modern shallow-marine
115 ecosystems due to the interplay between greenhouse gas-driven warming and
116 deoxygenation (Breitburg et al., 2018; Norris et al., 2013). Decreased gas solubility
117 and intensified ocean stratification may cause seawater deoxygenation under
118 greenhouse conditions, leading to the expansion of the oxygen minimum zone (OMZ)
119 in midwater and shoaling of its upper boundary to shallower depths; consequently, the
120 well-oxygenated habitat above the OMZ is vertically compressed (Breitburg et al.,
121 2018; Stramma et al., 2012; Stramma et al., 2010). Global expansion of low-oxygen
122 marine environments in conjunction with more extreme local seawater deoxygenation
123 have frequently accompanied major hyperthermal events including the PETM
124 (Dickson et al., 2012; Nicolo et al., 2010; Vellekoop et al., 2018). Through such
125 mechanisms, vertical migrations and local extinctions of shallow and midwater
126 marine biota driven by oxygen availability changes during extremely warm periods
127 like the PETM may be expected (Breitburg et al., 2018; Stramma et al., 2012;
128 Stramma et al., 2010).

129

130 **Material and Methods**

131 *Sample processing and data analysis*

132 The PETM sections of the SDB core (210.06-188.06 m core depth) were sub-
133 sampled at approximately 12 cm intervals, so that 124 sub-samples were analyzed for

134 their fossil ostracod contents. Carbon isotope values are after Self-Trail et al. (2012).
135 We adopted the standard sample processing method for ostracod research, i.e., we wet
136 sieved samples with mesh sizes of 63 μm then dry sieved with mesh size of 125 μm ,
137 after oven drying (Yasuhara et al., 2017a). Ostracods picked from the $>125 \mu\text{m}$
138 fraction are usually adults and late molt stage juveniles that can be confidently
139 identified (Yasuhara et al., 2017a). Each articulated carapace was counted as two
140 valves (Yasuhara et al., 2017a).

141 Non-metric multidimensional scaling (NMDS) analysis was performed to
142 understand the faunal turnovers related to climatic and oceanographic changes during
143 four stages around the PETM: pre PETM, peak PETM, recovery phase I and
144 recovery phase II. The NMDS analysis was based on three-point moving sums of
145 ostracod census data and low-abundance data points were excluded (number of valves
146 <10) to address the issues with low sample size (Yasuhara et al., 2008; Yasuhara et al.,
147 2014). The analysis was done using the R package ‘vegan’ (Oksanen et al., 2018),
148 using relative abundances of ostracod species and Bray-Curtis dissimilarity.

149

150 ***Estimation of local appearance and disappearance dynamics***

151 We carried out analyses of the raw ostracod fossil dataset based on the
152 Bayesian framework in the program PyRate (Silvestro et al., 2019; Silvestro et al.,
153 2014). We analyzed the datasets under time-varying birth-death models to
154 simultaneously estimate for each clade (i) the parameters of the preservation process,
155 (ii) the times of local speciation (T_s) and local extinction (T_e) of each ostracod species,
156 (iii) the speciation (λ) and extinction (μ) rates and their variation through time, and (iv)
157 the number, timing (= core depths as the surrogate) and magnitude of shifts in

158 speciation and extinction rates. While some methods can be sensitive to ghost
159 lineages (a.k.a. the Lazarus effect), the PyRate approach benefits from the estimation
160 of T_s and T_e of the studied species taking into account preservation biases, and thus
161 provides estimates of species' longevity (i.e., duration or time span of a species),
162 which therefore reduces the issues pertaining to the estimation of speciation and
163 extinction rates and so for the number of species through time (Silvestro et al., 2019;
164 Silvestro et al., 2014). For the purposes of this research, we consider T_s and T_e to
165 indicate appearance and disappearance, respectively, in the SDB core sediments and
166 not true speciation and extinction events. The preservation process infers the
167 individual origination and extinction times of each taxon based on all occurrences and
168 on an estimated preservation rate, denoted q , and expressed as expected occurrences
169 per taxon per meter. We applied a time-variable birth-death model that estimates rate
170 variations and infers shifts of diversification as well as the T_s and T_e for each species.
171 We first performed the classical BDMCMC (-A 2 option) (Silvestro et al., 2014) and
172 its recently enhanced version through the reversible-jump MCMC (RJMCMC)
173 algorithm (-A 4 option) (Silvestro et al., 2019), which allows an accurate estimate of
174 the speciation and extinction rate shifts.

175 We ran PyRate for 5 million MCMC generations with sampling frequency of
176 5,000 for the whole dataset. All analyses were set with the best-fit preservation
177 process after comparing (-PPmodeltest option) the homogeneous Poisson process (-
178 mHPP option), the non-homogeneous Poisson process (default option), and the time-
179 variable Poisson process (-q option). The time-variable Poisson process estimated a
180 preservation rate every 2 meters of sediments. We also accounted for varying
181 preservation rates across taxa using the Gamma model (-mG option), that is, with
182 gamma-distributed rate heterogeneity (Silvestro et al., 2014). We monitored chain

183 mixing and effective sample sizes by examining the log files in Tracer 1.7.1 (Rambaut
184 et al., 2018) after excluding the first 10% of the samples as the burn-in period. We
185 then combined the posterior estimates of the origination and extinction rates across all
186 replicates to generate rates-through-time plots (origination, extinction, and net
187 diversification) and the 95% credibility intervals (CI) of each rate.

188 We replicated all the analyses on ten randomized datasets and calculated
189 estimates of T_s and T_e as the mean of the posterior samples from each replicate. Thus,
190 we obtained ten posterior estimates of the T_s and T_e for all species and we estimated
191 the past diversity dynamics by calculating the number of living taxa at every point in
192 time based on the T_s and T_e . For all the subsequent analyses, we used the estimated T_s
193 and T_e for all species, which avoids re-modeling preservation and re-estimating times
194 of speciation and extinction, therefore focusing exclusively on the estimation of the
195 birth-death parameters for specific models. This procedure reduced drastically the
196 computational burden, while still allowing to account for the preservation process and
197 the uncertainties associated with the fossil ages.

198 To statistically identify a Lazarus taxon that has a range termination within the
199 peak PETM in the SDB core, we used the Bayesian birth-death model to show the 95%
200 confidence intervals of the disappearance and re-appearance horizons are not
201 overlapped within the peak PETM for a Lazarus taxon. We treated a Lazarus taxon as
202 two evolutionary entities in operation (e.g., *Hazelina1_pre* and *Hazelina1_post* for the
203 first and second appearance periods, respectively) in our Bayesian birth-death
204 modeling to fully reconstruct local extinction and speciation processes. By doing so,
205 we considered initial disappearances of Lazarus taxa at the PETM onset as local
206 extinction events and their subsequent re-appearances in the recovery phases as local
207 speciation events. We also showed the results of the original dataset in the online

208 supplementary material (i.e., treating a Lazarus taxon as one evolutionary entity, fig.
209 S1) for comparison.

210

211 **Oceanographic and geological setting**

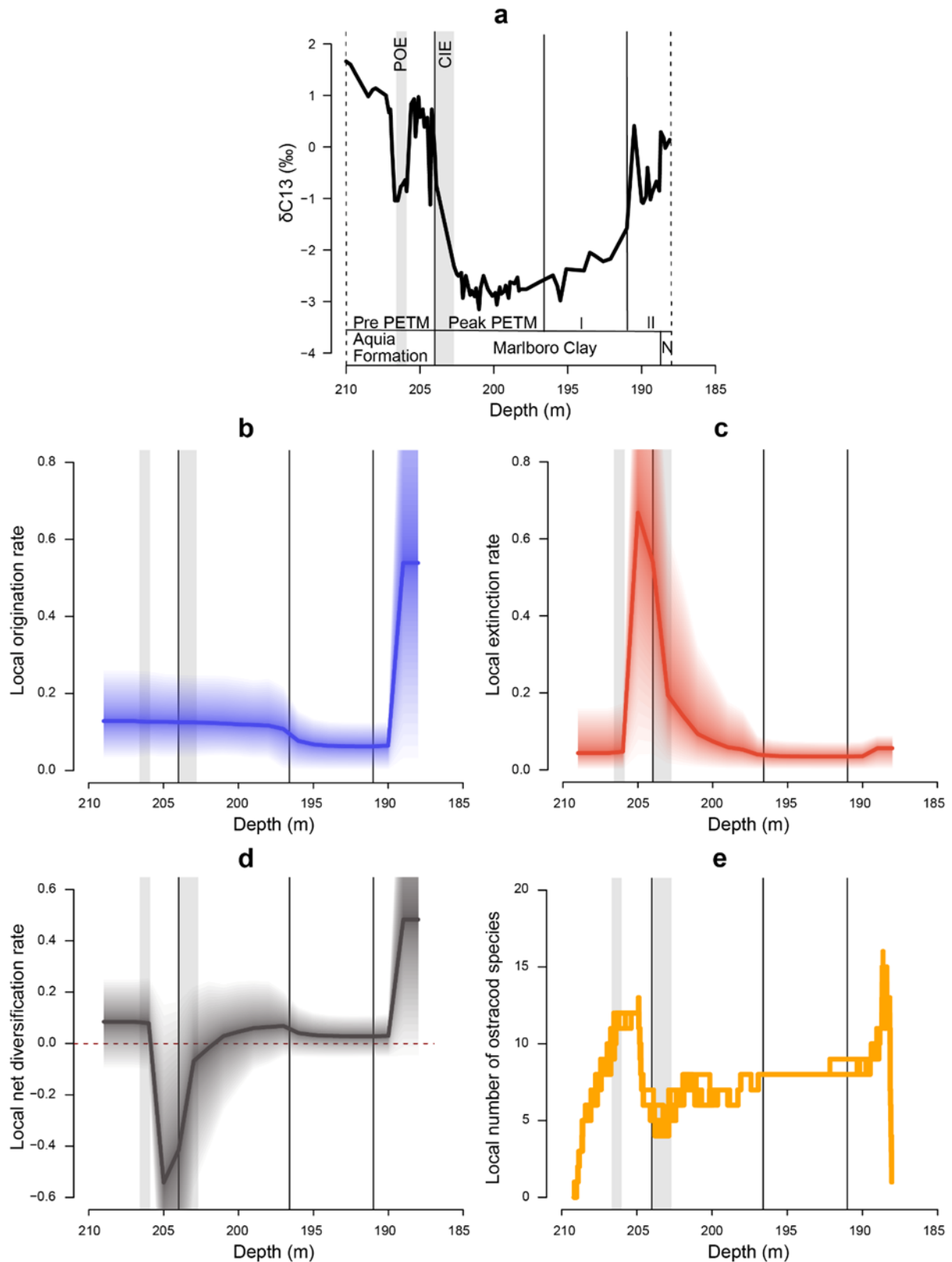
212 Highly-expanded sections of shallow marine PETM sediments (210.06–
213 188.06 m core depth) were obtained in the South Dover Bridge (SDB) core in the
214 Salisbury Embayment of the mid-Atlantic Coastal Plain in Maryland, USA
215 (38.74704° N; 76.00697° W) (Fig. 1) (Self-Trail, 2011; Self-Trail et al., 2012). The
216 Paleocene-Eocene boundary sequence of the SDB core consists of three depositional
217 units: the upper Paleocene Aquia Formation (210.06–204 m), the lower Eocene
218 Marlboro Clay (204–188.4 m) and the lower Eocene Nanjemoy Formation (188.4–
219 188.06 m) (Self-Trail et al., 2012). In the Aquia Formation, a pre-onset excursion
220 (POE: 206.6-205.9 m) is marked by a 2‰ negative shift in bulk $\delta^{13}\text{C}$ and partial
221 dissolution of benthic calcareous fossils (Fig. 2a) (Robinson and Spivey, 2019). The
222 contact between the Aquia Formation and the overlying Marlboro Clay at 204 m
223 corresponds to the base of the CIE with a rapid 3-4‰ negative shift in bulk $\delta^{13}\text{C}$ over
224 a 1.3-m dissolution zone, which marks the onset of the PETM (Fig. 2a). This 1.3-m
225 dissolution zone (204-202.7 m) at the base of the Marlboro Clay with trace amount of
226 calcareous fossils is most likely caused by the shoaling of the lysocline to the middle
227 shelf in the Salisbury Embayment, coinciding with the rapid CIE onset (Fig. 2a)
228 (Bralower et al., 2018; Self-Trail et al., 2012).

229 Based on lithological analyses, calcareous nannofossils and the carbon isotope
230 signal (Self-Trail, 2011; Self-Trail et al., 2012), we further divide the Paleocene-
231 Eocene boundary sequence into four sections corresponding to different stages of

232 PETM development: pre PETM (Aquia Formation, 210–204 m), peak PETM (lower
233 Marlboro Clay, 204–196.6 m), recovery phase I (middle Marlboro Clay, 196.6–191
234 m), and recovery phase II (upper Marlboro Clay and Nanjemoy Formation, 191–188
235 m) (Fig. 2a). The PETM onset, peak and initial recovery are nearly, if not entirely,
236 complete in terms of sedimentary sequence. Nannofossil biostratigraphy indicates
237 some missing time (<0.9 My) at the Aquia/Marlboro Clay contact (and none at the
238 Marlboro Clay/Nanjemoy contact) (Self-Trail et al., 2012), but this hiatus is most
239 likely restricted to the upper Aquia Formation, as the basal Marlboro Clay contains
240 the dissolution zone that accompanies the PETM-onset acidification event (Self-Trail
241 et al., 2012). The only disconformity within PETM sediments is situated at the top of
242 the calcareous nannofossil zone NP10 at 188.05 m (Self-Trail et al., 2012) at the very
243 top of our study interval, which therefore has no effect on our discussion.

244 SDB sediments were deposited at subtropical to temperate paleolatitude, in an
245 environment with seasonal water temperature changes (León y León et al., 2018; Self-
246 Trail et al., 2012). Planktic and benthic foraminiferal data from SDB samples indicate
247 a water depth of ~125 m prior to the PETM onset and ~140 m after the PETM onset
248 (Robinson and Spivey, 2019). While uncertainties and disagreements among PETM
249 water depth proxies in the Salisbury Embayment remain (Stassen et al., 2014),
250 reconstructions based on benthic foraminifer assemblage data agree that sea level may
251 have risen by as much as 30 m across the PETM onset (León y León et al., 2018;
252 Robinson and Spivey, 2019).

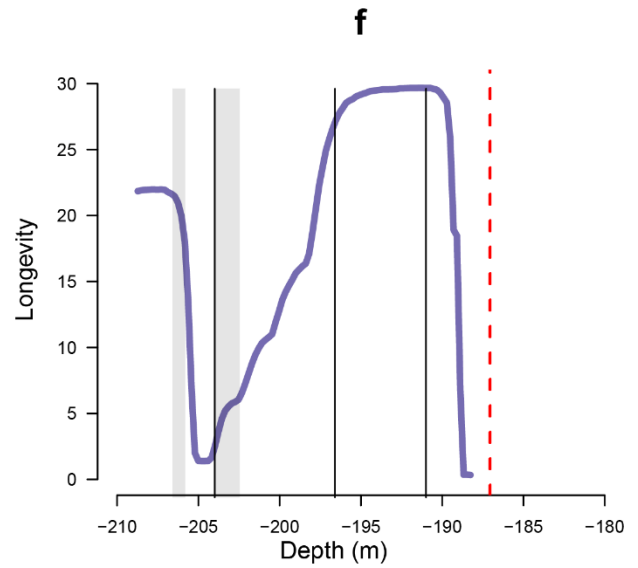
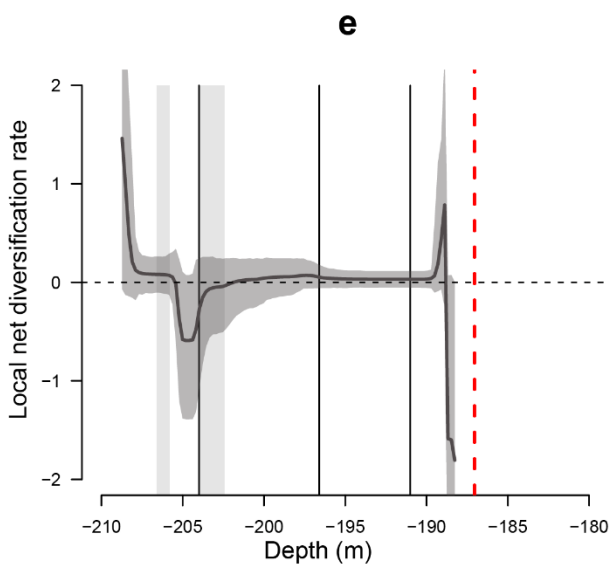
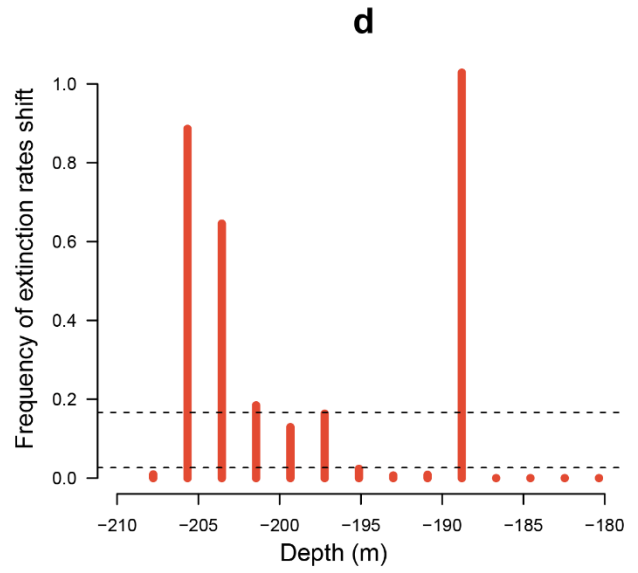
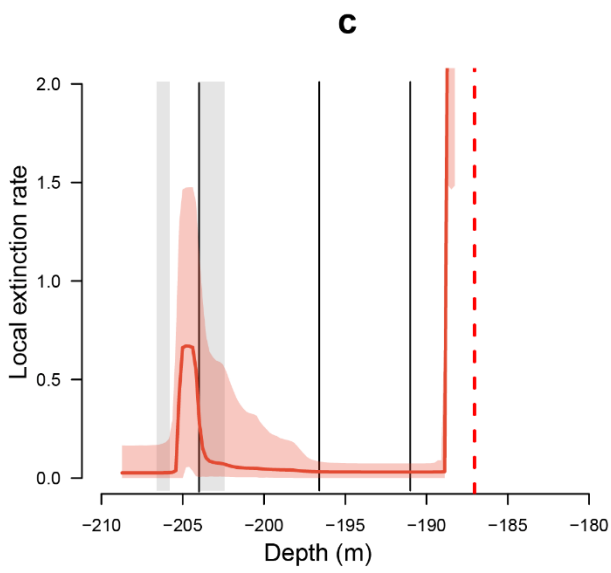
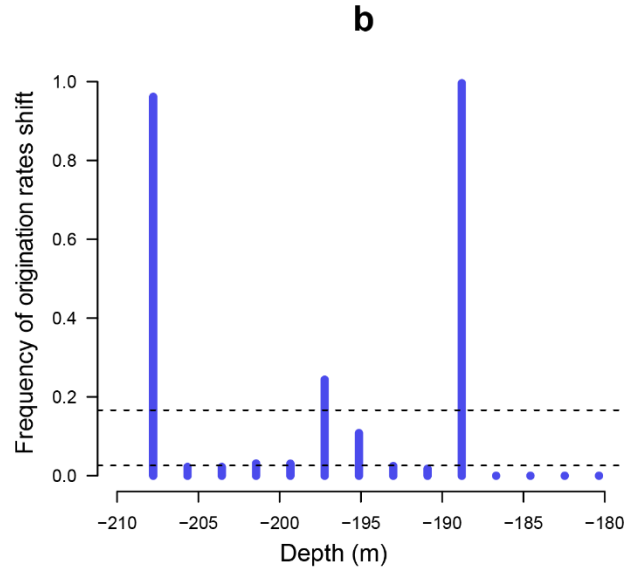
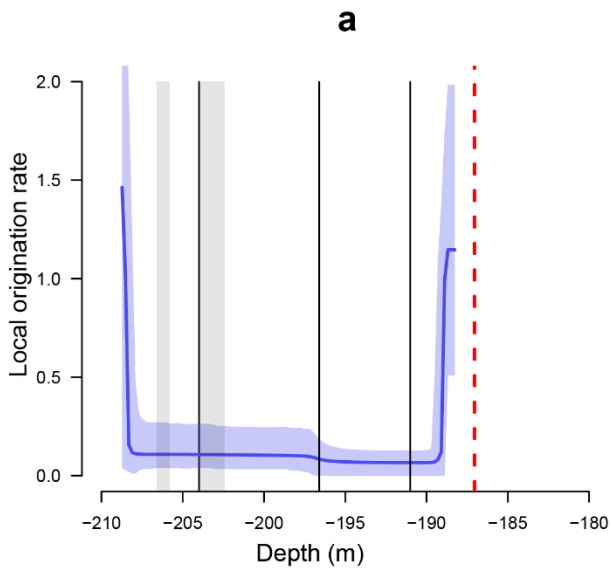
253



254 **Fig. 2.** Bayesian estimation of local diversity dynamics of the ostracod community
 255 across the PETM. Each Lazarus taxon is divided into two evolutionary entities of the
 256 pre-PETM section and post-PETM section. (a) The bulk $\delta^{13}\text{C}$ curve for comparison

257 (Self-Trail et al., 2012). Vertical dotted lines at 210 m and 188 m define the interval
258 of study. The division into pre PETM, peak PETM, recovery phase \square and recovery
259 phase \square is based on the carbon isotope baseline, excursion, initial recovery and final
260 recovery, respectively (\square for recovery phase \square and \square for recovery phase \square).

261 Depositional units of Paleocene/Eocene boundary section are shown in stratigraphic
262 order (N for Nanjemoy Formation). Grey bars at 206.6-205.9 m and 204-202.7 m
263 indicate the POE and the CIE onset, respectively. Inferences of **(b)** species appearance
264 rates and **(c)** species disappearance rates with the birth-death model. **(d)** The net
265 diversification rates as the difference between appearance and disappearance rates
266 (rates below 0 indicate declining diversity). Solid lines indicate mean posterior rates,
267 and the shaded areas show the 95% confidence interval. **(e)** The local ostracod
268 diversity trajectory. Note that the zero diversity at the beginning and ending of the
269 curve is an analytical artifact as the model assumes the lineages diversified from zero
270 and eventually went extinct (end of the core section).



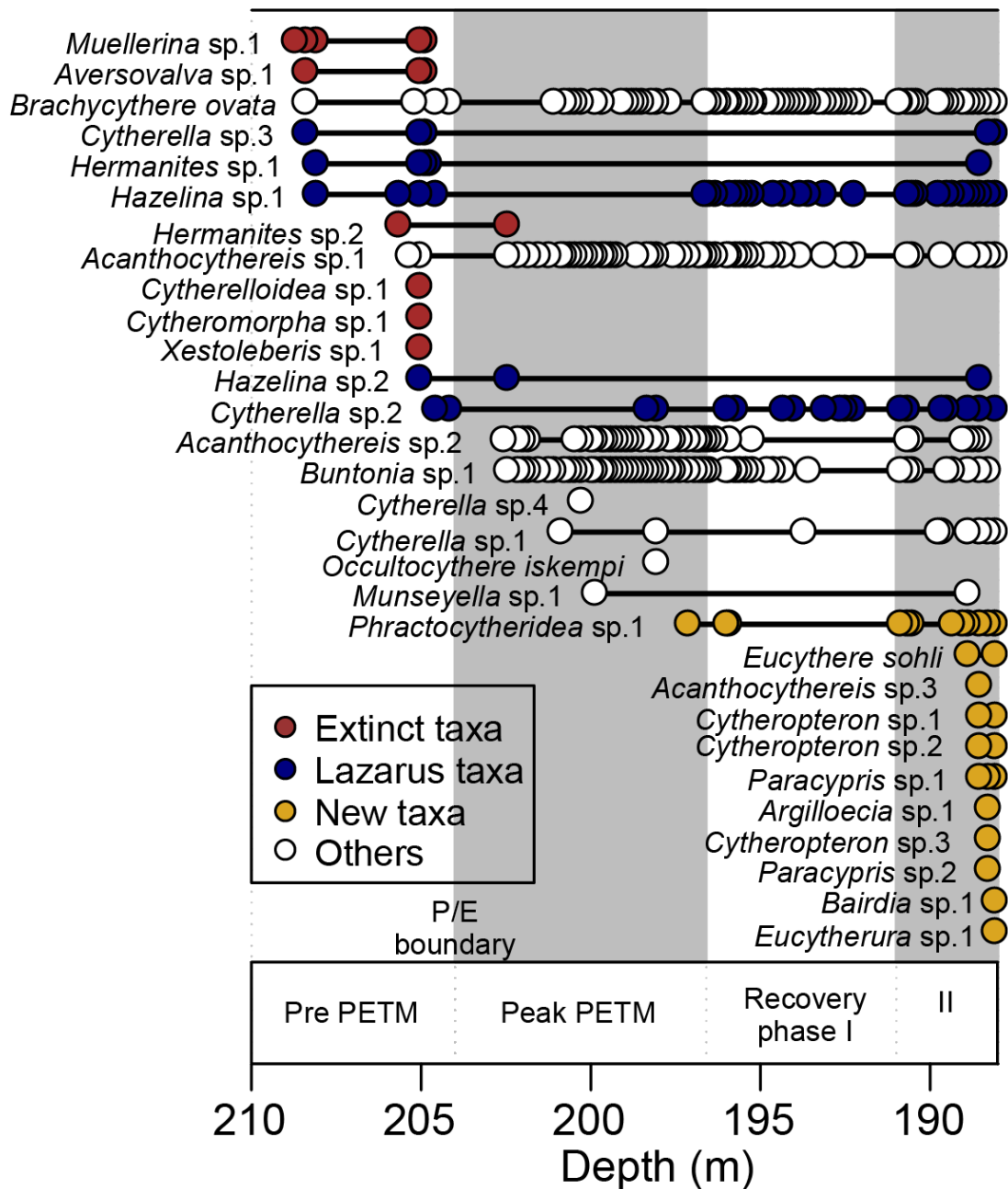
272 **Fig. 3.** Bayesian estimation of the local diversity dynamics of ostracod community
273 throughout the PETM using the RJMCMC model. Each Lazarus taxon is divided into
274 two evolutionary entities of the pre-PETM section and post-PETM section. Red
275 vertical dotted line at 188 m indicates the end of the core section. Black vertical lines
276 at 204 m, 196.6m, and 191 m indicate the division of the core section into pre PETM,
277 peak PETM, recovery phase □ and recovery phase □. Grey bars at 206.6-205.9 m and
278 204-202.7 m indicate the POE and the CIE onset, respectively. **(a)** The species
279 appearance rates. High rate at the beginning of the curve is an analytical artifact as the
280 model assumes the lineages diversified from zero. **(b)** The frequency of species
281 appearance rates shifts. Frequency > 0.167 (indicated by the upper dashed line) is
282 considered as significant shift (Bayes factor > 6). Significant shift at 207.78 m is
283 likely an analytical artifact. **(c)** The species disappearance rates. High rate at the
284 ending of the curve is an analytical artifact as the model assumes the lineages
285 eventually went extinct. **(d)** The frequency of species disappearance rates shifts.
286 Frequency > 0.167 (indicated by the upper dashed line) is considered as significant
287 shift (Bayes factor > 6). Significant shift at 188.79 m is likely an analytical artifact. **(e)**
288 The net diversification rates as the difference between species appearance and
289 disappearance rates (rates below 0 indicate declining diversity). Solid lines indicate
290 mean posterior rates and the shaded areas show 95% CI. **(f)** The mean longevity of
291 ostracod lineages. Note that the zero longevity at the ending of the curve is an
292 analytical artifact as the model assumes the lineages eventually went extinct (end of
293 the core section).

294

295 **Results**

296 ***Bayesian process-based birth-death model***

297 We analyzed the SDB ostracod fossil record throughout the PETM (1210
298 specimens, 30 species, 122 samples in total) using a Bayesian process-based birth-
299 death model considering time-variable preservation rates (Zizka et al., 2019). We
300 successfully reconstructed the changes in species appearance and disappearance rates
301 throughout the PETM and its recovery phases in unprecedented detail (Figs. 2 and 3).
302 When estimating the local preservation rates for time bins as represented by 2-m
303 stratigraphic layers, the results clearly demonstrate a time-variable preservation
304 process ranging from 0.037 to 20.58 occurrences per lineage per meter core depth in
305 the POE (q1) and the recovery phase II (q10), respectively (table S1). Importantly, the
306 model estimated a significant shift in species appearance rates at 188.79 m, indicating
307 rapid origination at the end of the PETM (Figs. 2b and 3a-b); it also estimated
308 significant shifts in species disappearance rates at 205.67 m and at 203.56 m with a
309 strong peak between ~205-204 m (Figs. 2c and 3c-d). The net diversification rate
310 indicated a drastic diversity decline initiated at ~206 m (POE) with local diversity
311 dropping from 13 to 5 species during the PETM onset, followed by a slight partial
312 recovery at ~200 m enforced by a local turnover (*i.e.* appearance equal to
313 disappearance), and a final strong boost in the recovery phase II leading to a local
314 diversity increase from 9 to 16 species (Fig. 2, d and e). Simple presence/absence data
315 gives consistent results that 6 out of 13 pre-PETM species were permanently
316 eliminated from the local assemblages at the PETM onset (46.2% disappearance), and
317 another 5 out of 13 pre-PETM species disappeared during the peak PETM and re-
318 appeared during recovery phases (38.5% Lazarus taxa); on the other hand, 11 out of
319 22 recovery-phase species first appeared only after the peak PETM (50% new
320 appearance) (Fig. 4).



321

322 **Fig. 4.** Occurrence ranges of all ostracod species. Each dot indicates species presence
 323 in the sample. Extinct pre-PETM taxa that do not extend beyond the PETM onset,
 324 Lazarus pre-PETM taxa that have range terminations within the peak PETM, and
 325 newly occurring post-PETM taxa are highlighted by red, blue, and yellow,
 326 respectively. Peak PETM and recovery phase II are shaded by gray (□ for recovery

327 phase □). For all Lazarus taxa, the 95% confidence intervals of the disappearance and
328 re-appearance horizons are not overlapped (table S1).

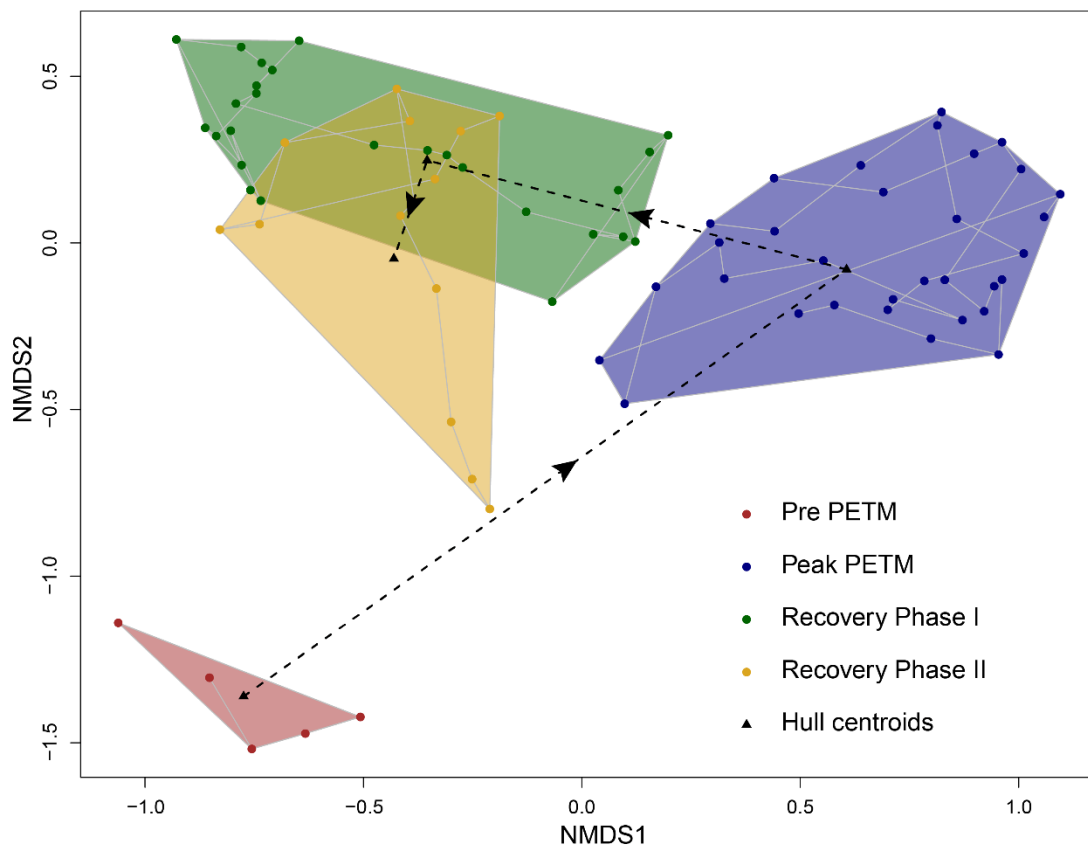
329

330 *NMDS analysis*

331 The non-metric multidimensional scaling (NMDS) analysis shows that
332 samples from each of the four study intervals (*i.e.*, pre-PETM, peak PETM, recovery
333 phase I and recovery phase II) cluster in two-dimensional space (Fig. 5). The pre-
334 PETM assemblage is most distinguished from all other assemblages, especially from
335 the peak-PETM assemblage, based on their relative positions in NMDS space (Fig. 5),
336 indicating a conspicuous ostracod faunal transition at the PETM onset. From the peak
337 PETM to recovery phase I and then phase II, the three assemblages become
338 progressively more similar to the pre-PETM assemblage in NMDS space with the two
339 recovery assemblages partially overlapping (Fig. 5). Approaching the end of the
340 PETM, the position of recovery phase □ in-between peak-PETM and pre-PETM
341 assemblages indicates a partial recovery of the ostracod community (*i.e.*, reoccurrence
342 of 5 Lazarus taxa) besides some imprints of remanent peak-PETM faunal elements
343 and first occurrence of post-PETM faunal elements.

344 Indeed, the down-core trend of NMDS axis 2 values is clearly opposite to that
345 of $\delta^{13}\text{C}$ (Fig. 6), representing the elimination and recovery process of the pre-PETM
346 type fauna. The peak-PETM and recovery phase □ fauna have much higher NMDS
347 axis 2 values compared with the pre-PETM fauna, corresponding to the ‘body’ of the
348 CIE with relatively stable and low $\delta^{13}\text{C}$ values (Fig. 6). The recovery phase □ fauna
349 quickly decline in the NMDS axis 2 towards the end of the PETM in contrast with the
350 exponential recovery of $\delta^{13}\text{C}$ to pre-PETM values (Fig. 6). On the other hand, the

351 down-core trend of NMDS axis 1 values represents the peak PETM fauna, showing
352 highest values between ~202-197 m core depth (Fig. 6). Our high-time resolution
353 down-core NMDS data revealed three distinct, successive maxima in the peak PETM
354 fauna (Fig. 6) indicating repeated small biotic perturbations during the peak PETM.
355



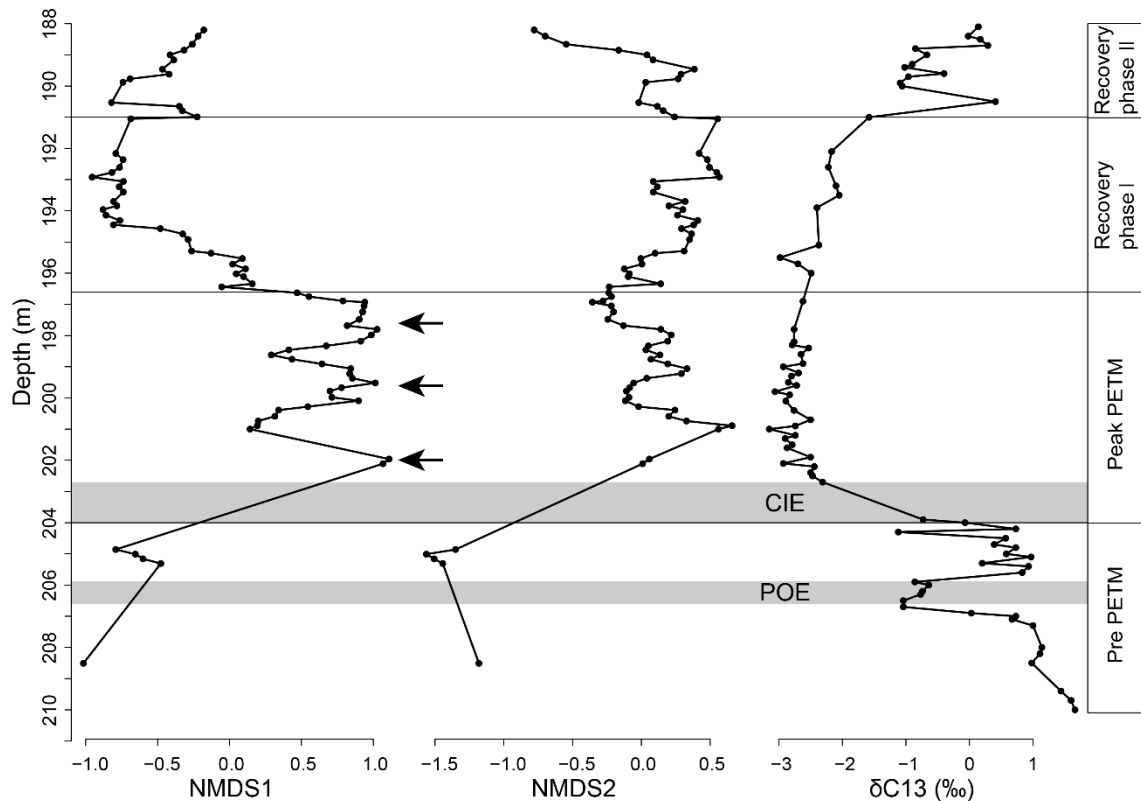
356
357 **Fig. 5.** Non-metric Multidimensional Scaling result showing the PETM-associated
358 faunal changes. Three-point moving sums of ostracod census data are used for the
359 NMDS analysis. Four stratigraphic groupings: pre-PETM (red); peak-PETM (blue);
360 recovery phase I (green); and recovery phase II (yellow). The grey lines connect one
361 sample to the next in stratigraphic order within each group. Black dashed lines
362 connecting the hull centroid of each group indicate ostracod faunal transitions across
363 the PETM in NMDS space.

364

365

366

367



368 **Fig. 6.** Down-core NMDS axis 1 and NMDS axis 2 scores compared to the bulk $\delta^{13}\text{C}$

369 curve. Three-point moving sums of ostracod census data are used for the NMDS

370 analysis. Arrows indicate distinct maxima in the peak PETM fauna at ~202 m, 200 m,

371 and 198 m along the NMDS axis 1, respectively. Grey bars at 206.6-205.9 m and 204-

372 202.7 m indicate the POE and the CIE onset, respectively.

373

374 Discussion

375 *Disruption and recovery of ostracod community throughout the PETM*

376 We detect significant local disappearance from the pre PETM to the CIE onset
377 in metazoan shallow-marine benthos by the Bayesian process-based birth-death model
378 (Fig. 2). Even if we do not consider a Lazarus taxon as two operational evolutionary
379 entities in the modeling, this disappearance remains significant albeit weaker (*i.e.*,
380 permanent extirpation of 6 non-Lazarus pre-PETM taxa) (table S2 and fig. S1),
381 indicating that a part of this species disappearance event accounted for unrecoverable
382 biodiversity loss in the shallow-marine benthic ecosystem. The disappearance peak
383 indicated by the birth-death model slightly pre-dates the CIE onset, which may reflect
384 the extinction started at the POE as a precursor to the main hyperthermal event.
385 Similarly, planktic and benthic foraminifera also showed assemblage changes in terms
386 of faunal composition at SDB and nearby sites prior to the CIE onset (Robinson and
387 Spivey, 2019). Early onset of PETM-associated biotic and environmental changes is
388 not confined to the Salisbury Embayment but also evident in the New Jersey shelf,
389 southwest Pacific Ocean and North Sea (León y León et al., 2018; Sluijs et al., 2007b),
390 consistent with our understanding of the destabilization of ocean-atmosphere system
391 preceding the PETM resulting in perturbed and stressful water conditions. Abrupt
392 local disappearance at the PETM onset may be associated with species habitat range
393 shifts/contraction in response to peak-PETM ecological and environmental stress, and
394 not necessarily global extinction. Recovery and diversification at the end of PETM
395 was unexpectedly strong (*i.e.*, reappearance of 5 Lazarus taxa and first appearance of
396 11 post-PETM taxa), regardless of the treatment of the Lazarus taxa in the modeling
397 (Fig. 2; fig. S1; table S1 and S2). This post-PETM biodiversity pattern is also evident
398 in earlier studies of benthic biotic response. Ostracod fauna of the Tethyan region
399 show similar recovery in diversity (Yamaguchi and Norris, 2012). Likewise, the
400 Atlantic Coastal Plain mollusks show elevated post-PETM diversity (Ivany et al.,

401 2018). Indeed, the PETM has been demonstrated to be an origination event in

Genus	Autoecology	References
-------	-------------	------------

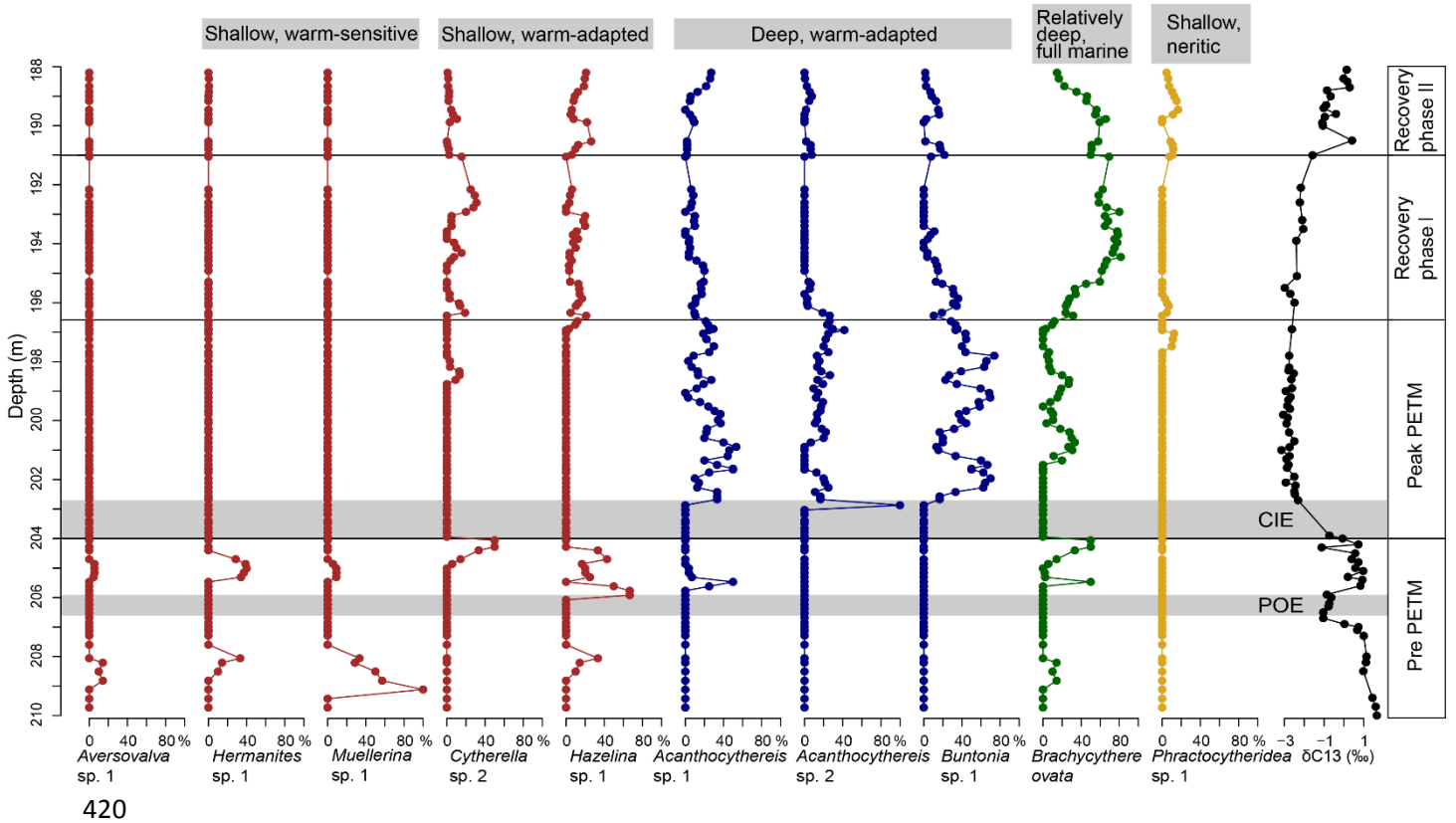
402 shallow-marine systems (Speijer et al., 2012). The birth-death model therefore clearly
403 reveals a perturbation-recovery pattern of the shallow-marine ecosystem characterized
404 with one peak of species disappearance predating the PETM onset and the other peak
405 of species reappearance combined with first appearance at the final recovery phase.
406 NMDS analysis consistently shows that the greatest faunal turnover occurred at the
407 PETM onset followed by a gradual, partial return of pre-PETM faunal elements and
408 first occurrence of post-PETM faunal elements during the recovery phases such that
409 the ostracod community approached a new state in terms of species composition after
410 the PETM transition (Figs. 5 and 6). Irreversible impacts of climate change on the
411 benthic ecosystem are represented by the difference between recovery phase II and
412 pre-PETM assemblages in the NMDS space. To interpret such shallow-marine biotic
413 responses to the PETM, we suggest deoxygenation and warming during the PETM
414 (see discussion below) may have reset the species assemblages and opened up niches
415 for new colonization both from shallower and deeper depths, resulting in local
416 diversification and possibly true speciation.

417

<i>Acanthocythereis</i>	Deep (outer neritic to bathyal), warm-adapted (i.e., typical warm Paleogene genus), full marine, epifauna (low-oxygen-sensitive)	(Huang et al., 2018; Huff, 1970)
<i>Brachycythere</i>	Relatively deep (outer neritic), full marine	(Huff, 1970; Morkhoven, 1962)
<i>Buntonia</i>	Deep (outer neritic to bathyal), warm-adapted (i.e., typical warm Paleogene genus), full marine, epifauna (low-oxygen-sensitive)	(Huff, 1970; Morkhoven, 1962; Yasuhara et al., 2016; Yasuhara et al., 2015)
<i>Cytherella</i>	Shallow (neritic), warm-adapted (i.e., typical tropical genus), full marine	(Morkhoven, 1962; Shin et al., 2019; Yamaguchi et al., 2014; Yasuhara et al., 2015)
<i>Hazelina</i>	Shallow (neritic), warm-adapted (i.e., typical warm Paleogene genus), full marine	(Huff, 1970; Lord et al., 2009; Van Nieuwenhuise, 2007)
<i>Hermanites</i>	Shallow (inner neritic), warm-sensitive (i.e., common in extratropical areas), full marine	(Cronin, 1991; Lord et al., 2009; Morkhoven, 1962; Van Nieuwenhuise, 2007)
<i>Muellerina</i>	Shallow (neritic), warm-sensitive (i.e., typical cold Neogene and extratropical genus), full marine	(Cronin, 1991; Wood and Whatley, 1997; Yasuhara et al., 2019)
<i>Phractocytheridea</i>	Shallow (inner neritic), brackish	(Morkhoven, 1962; Puckett, 1994)

418 Table 1. Autoecology summary of important genera.

419



421 **Fig. 7.** Three-point moving summed relative abundance plots of common and
 422 ecologically significant ostracod species compared against the bulk $\delta^{13}\text{C}$ curve.
 423 Characteristic species of the pre-PETM, peak-PETM, recovery phase I and recovery
 424 phase II are highlighted by corresponding color used in Figure 5 with their
 425 environmental preferences shown on the top (see Table 1 for details). Grey bars at
 426 206.6-205.9 m and 204-202.7 m indicate the POE and the CIE onset, respectively.

427
 428 ***Biotic response to paleoceanographic changes: sea-level rise, elevated warmth and***
 429 ***OMZ expansion***

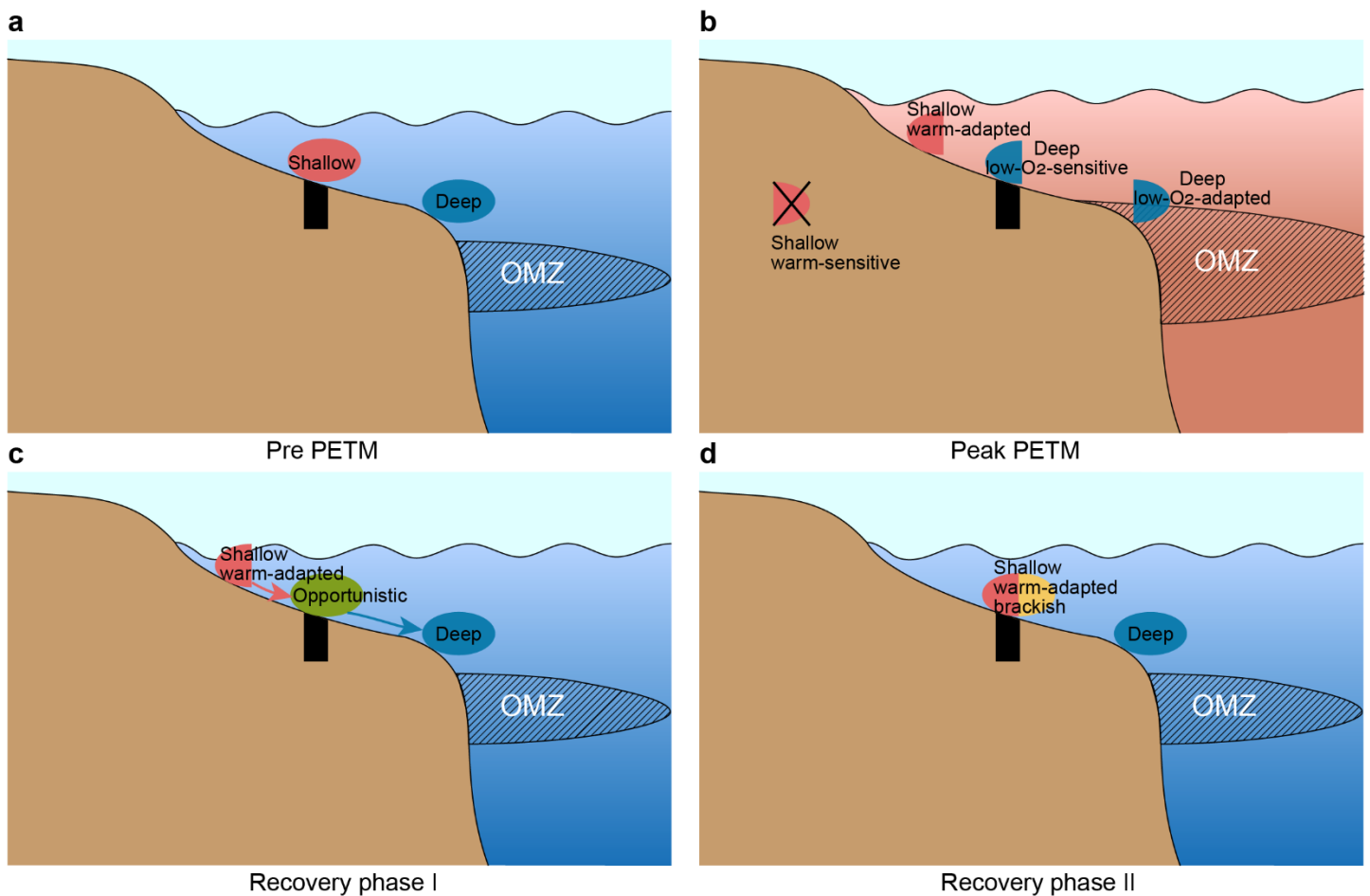
430 The disruption-recovery pattern of the ostracod community indicated by birth-
 431 death model and NMDS analysis can be better understood by examining faunal
 432 turnovers across the PETM in detail through changes in the relative abundance of

433 common and ecologically significant species across the late Paleocene-early Eocene
434 time series (Table 1; Fig. 7). We consider the pre-PETM assemblage to represent the
435 ecological and environmental baseline for the region. During the pre PETM,
436 *Aversovalva*, *Brachycythere*, *Cytherella*, *Hazelina*, *Hermanites* and *Muellerina*
437 sporadically attain high relative abundance. Most species of the pre-PETM
438 assemblage inhabited shallow-marine environments (neritic zone) , but they had
439 different thermal tolerances as indicated by their latitudinal distribution ranges (i.e.,
440 extratropical [=sensitive] or tropical [=adapted] taxa) : *Hermanites* and *Muellerina* are
441 warm-sensitive genera, whereas *Cytherella* and *Hazelina* are warm-adapted genera
442 (Table 1) (Cronin, 1991; Huff, 1970; Lord et al., 2009; Morkhoven, 1962; Shin et al.,
443 2019; Van Nieuwenhuise, 2007; Wood and Whatley, 1997; Yamaguchi et al., 2014;
444 Yasuhara et al., 2019; Yasuhara et al., 2015). During the peak PETM, characteristic
445 species of the pre-PETM assemblage either completely extirpated (*Aversovalva* and
446 *Muellerina*, extinct taxa) or temporarily disappeared (*Cytherella*, *Hermanites* and
447 *Hazelina*, Lazarus taxa). The genera *Acanthocythereis* and *Buntonia* dominated the
448 peak-PETM assemblage instead (Figs. 4 and 7). They show ecological affinities to
449 much greater water depths (outer neritic-bathyal zone) and possibly adapted to
450 elevated warmth as they are very common, widespread genera throughout the
451 Paleocene/Eocene greenhouse period (Table 1) (Huff, 1970; Morkhoven, 1962;
452 Yasuhara et al., 2015). Such abrupt faunal turnovers from the pre to peak-PETM are
453 represented as major perturbations/excursions of the ostracod community associated
454 with peak-PETM paleoceanographic conditions. Relative abundances of peak-PETM
455 taxa rapidly decreased at the transition from the peak PETM to recovery phase I,
456 coeval with a dramatic increase of *Brachycythere* as a relatively deep and fully marine
457 opportunistic taxon (Huff, 1970; Morkhoven, 1962) and a slight increase of Lazarus

458 taxa (Table 1; Figs. 4 and 7). During recovery phase II, the Lazarus taxa reached
459 moderately high abundances (20-40%) while the recovery phase I taxon
460 *Brachycythere* gradually declined towards the end of PETM; *Phractocytheridea* as a
461 newly occurring post-PETM taxon that inhabited shallow brackish environments
462 (Morkhoven, 1962; Puckett, 1994) made its first consistent appearance (Table 1; Fig.
463 7). The assemblage of recovery phase II therefore has high diversity and low
464 dominance with the return of Lazarus taxa and the first occurrence of post-PETM taxa
465 (Figs. 4 and 7), corresponding to the recovery and diversification of the ostracod
466 community when pre-PETM climatic and paleoceanographic conditions resumed
467 (McInerney and Wing, 2011). In addition to above-discussed faunal turnovers, it is
468 noticeable that several taxa (e.g., *Acanthocythereis* and *Brachycythere*) survived
469 throughout the PETM (Fig. 4)

470 The replacement of the pre-PETM shallow assemblage by the peak-PETM
471 deep, warm-adaptive assemblage is consistent with our background understanding of
472 sea-level rise associated with this hyperthermal event in the Salisbury Embayment
473 (Norris et al., 2013; Robinson and Spivey, 2019; Sluijs and Brinkhuis, 2009; Sluijs et
474 al., 2008; Zachos et al., 2006). In addition, the peak-PETM assemblage includes
475 epifaunal forms sensitive to low-oxygen conditions and lack any infaunal forms
476 typically found at outer neritic-bathyal water depths during the Paleocene-Eocene
477 period, such as *Krithe*, that are adapted to low-oxygen-conditions (Huang et al., 2018;
478 Yamaguchi and Norris, 2012; Yasuhara et al., 2016). We interpret the intrusion of
479 deep, epifaunal (low-oxygen-sensitive) taxa into the SDB site as their upslope
480 migration to avoid the prevalence of low-oxygen conditions, due to OMZ expansion,
481 in deeper waters. In fact, oxygen depletion is one of the most well recognized
482 characteristics of the PETM greenhouse ocean (Breitburg et al., 2018; Gilly et al.,

483 2013; Norris et al., 2013; Sluijs et al., 2014; Winguth et al., 2012). The expansion of
 484 the OMZ in the PETM North Atlantic basin has been revealed by a regional ocean
 485 model simulation that a severely hypoxic condition inhospitable for many organisms
 486 prevailed on the continental slope below ~200 m while the middle and outer shelf
 487 underwent comparatively much milder decline in bottom water oxygenation (Hantsoo
 488 et al., 2018), consistent with micropaleontologic evidence of benthic foraminifera in
 489 the Salisbury Embayment (Robinson and Spivey, 2019; Self-Trail et al., 2017; Stassen
 490 et al., 2015).



491

492 **Fig. 8.** Cartoon showing the biotic responses to changes in sea level, water
 493 temperature and dissolved oxygen concentration across the PETM. Black bar: SDB
 494 core site; hashed area: OMZ, oxygen minimum zone; red circle: shallow taxa; blue

495 circle: deep taxa; green circle: opportunistic taxa; yellow circle: post-PETM shallow
496 taxa; X: extinction; arrows: downslope migration; blue background: cooler water
497 temperature; orange background: warmer water temperature. **(a)** Pre-PETM setting.
498 **(b)** During the peak PETM, deep, low-oxygen-sensitive taxa migrated upslope to the
499 outer neritic SDB site. Intrusion of deep, low-oxygen-sensitive taxa in concert with
500 sea-level rise forced shallow taxa to migrate upslope to extremely warm inner neritic
501 area, where warm-adapted taxa survived and warm-sensitive taxa went regionally
502 extinct. **(c)** As temperatures cooled and the OMZ constricted during recovery phase I,
503 deep, low-oxygen-sensitive taxa returned to deeper waters, and opportunistic taxa
504 thrived at the SDB site. **(d)** In recovery phase II, shallow, warm-adapted taxa re-
505 occupied the SDB site, and post-PETM shallow taxa occupied vacant ecological
506 niches left by the extinction of warm-sensitive taxa.

507

508 As illustrated in Figure 8a–b, when the depositional environment at the SDB
509 site changed from an inner-middle neritic setting to an outer neritic setting because of
510 sea-level rise (Robinson and Spivey, 2019), benthic ostracods, perhaps except deep
511 low-oxygen-adapted taxa (see below), migrated upslope to maintain their preferred
512 depth habitat ranges. Deep, low-oxygen-sensitive taxa may have migrated close to or
513 beyond the shallow limit of their preferred depth range, to the SDB site, to escape the
514 expanded OMZ since the severely hypoxic bathyal OMZ waters were not habitable
515 for them (Gilly et al., 2013; Hantsoo et al., 2018; Huang et al., 2018; Norris et al.,
516 2013; Winguth et al., 2012). Deep, low-oxygen-adapted taxa could have remained in
517 the deeper bathyal zone.

518 In other words, we propose that habitats of the deep, low-oxygen-sensitive
519 taxa were compressed from the outer neritic-bathyal zones to only the outer neritic
520 layer, a refugium from the expanded OMZ that covered broad bathyal depths in the
521 North Atlantic basin (Hantsoo et al., 2018). The intrusion of deep, low-oxygen-
522 sensitive taxa to the SDB site might have narrowed the ecological niches of the
523 shallow pre-PETM taxa. In conjunction with migration due to sea level rise, this
524 intrusion forced the entire shallow pre-PETM assemblage toward super warm surface
525 waters (Winguth et al., 2012; Zachos et al., 2006) upslope from SDB. Extreme surface
526 warming in the Salisbury Embayment is well documented by previous geochemical
527 and paleoecological studies (León y León et al., 2018; Self-Trail et al., 2012), causing
528 great perturbation of the shallow-marine ecosystem as represented by dramatic faunal
529 turnovers of planktic and benthic foraminifera and malformation of calcareous
530 nannoplankton during the PETM (Bralower and Self-Trail, 2016; Robinson and
531 Spivey, 2019). Among the shallow pre-PETM ostracod taxa leaving the SDB site,
532 only those tolerant to the warmer conditions were able to survive (Fig. 8b). Warm-
533 sensitive pre-PETM taxa could neither survive the elevated warmth of subtropical-
534 temperate surface waters, or escape to higher latitudes as these might be similarly
535 warm due to the flattened latitudinal temperature gradients in anomalous greenhouse
536 conditions (Zachos et al., 2006; Zhang et al., 2019). Such extreme thermal pressure
537 could have driven warm-sensitive taxa to at least regional extinction without cool and
538 shallow suitable habitats or refugia in high-latitude areas. Collectively, we infer that
539 extreme warming in the neritic environment and deoxygenation in the bathyal
540 environment in concert caused the ostracod faunal turnovers from the pre-PETM to
541 peak-PETM. Likely permanent extinction of six warm-sensitive pre-PETM taxa (Fig.
542 4) indicates that the impacts of habitat compression induced by warming and

543 deoxygenation might be irreversible, and the PETM as a transient hyperthermal event
544 punctuated long-term evolution of benthic organisms.

545 As peak-PETM conditions ended with the initial CIE recovery, *Brachycythere*
546 as a relatively deep opportunistic taxon temporarily achieved high dominance at the
547 SDB site during recovery phase I (Table 1; Figs. 7 and 8c). We propose that shallow,
548 warm-adapted taxa (*Cytherella* and *Hazelina*) and deep, low-oxygen-sensitive taxa
549 (*Acanthocythereis* and *Buntonia*) migrated downslope from their peak-PETM
550 positions to their pre-PETM positions during recovery phases I and II as temperatures
551 cooled, the OMZ constricted, and sea level fell (Fig. 8, c and d) (Self-Trail et al., 2012;
552 Sluijs and Brinkhuis, 2009). Overall paleoceanographic conditions might not have
553 fully recovered until shallow, warm-adapted Lazarus taxa eventually recolonized the
554 SDB habitat during recovery phase II (Figs. 4 and 8d). As the other shallow, warm-
555 sensitive pre-PETM taxa went extinct due to the unavailability of cooler refugia (Figs.
556 4 and 8b), vacant ecological niches left by them were occupied by newly occurring
557 post-PETM taxa like *Phractocytheridea*, a shallow brackish taxon (Table 1; Figs. 4
558 and 8d).

559 Interestingly, some deep-water indicator taxa also sporadically appeared in the
560 recovery phase II assemblage in very low abundances (e.g. *Acanthocythereis*,
561 *Cytheropteron*, and *Paracypris*) (Figs. 4 and 7) (Huff, 1970; Morkhoven, 1962).
562 Coexistence of shallow (inner-middle neritic) and deep (bathyal) ostracods is
563 uncommon in the modern icehouse ocean, as ostracods exhibit strong depth zonation
564 (Yasuhara et al., 2017b). Taphonomic effects of downslope contamination may
565 account for minor appearances of shallow species at a deeper site, but it would not
566 lead to dominance of the shallow species (Kidwell and Holland, 2002). Thus we tend
567 to prefer the ecological explanation that niche constraints (i.e., deep and shallow

568 separation) might be overcome in the unusual greenhouse ocean of the early Eocene
569 before the establishment of near-modern ocean circulation and vertical structure
570 (Hutchinson et al., 2019), which may explain the rapid and strong diversification at
571 the end of the PETM identified in the birth-death modeling.

572

573 **Conclusions**

574 In summary, this four-stage ostracod faunal turnover clearly reflects biotic
575 responses to paleoclimatic and paleoceanographic changes associated with the onset,
576 peak, initial recovery and final recovery of the PETM. Extreme warmth and OMZ
577 expansion as two prominent ecological stressors of the peak PETM together
578 controlled the extirpation and bathymetrical migration of ostracod species by
579 compressing available physical habitats. While upslope migration offers refugia to
580 species with wide depth range habitats, species unable to escape higher temperatures
581 and/or an expanded OMZ are forced to extirpation. Importantly, the PETM offers an
582 example of a threshold event where the recovered shallow shelf benthic community is
583 unlike the one that existed before the ecological collapse. Ostracod (seed shrimp)
584 faunal turnovers throughout the PETM could represent broader metazoan marine
585 benthic community responses and complete the big picture of PETM biotic changes
586 on the shallow shelf in concert with the foraminifera and nannofossil data, which
587 eventually provide a potential analog to future scenarios of short-term and long-term
588 biotic changes in relevance to anthropogenic warming in a greenhouse world.

589

590 **Data accessibility statement**

591 All data supporting this article has been uploaded as part of the Supplementary
592 Materials and will be deposited in Pangaea (DOI will be added later).

593

594 **Acknowledgments**

595 We thank Maria Lo and Rachel Wong for their assistance in the laboratory; Maoyan
596 Zhu, Jed O. Kaplan, and Timothy Horscroft for editorial helps; and Thomas M.
597 Cronin, Jean M. Self-Trail, Marie-Béatrice Forel and an anonymous reviewer for
598 valuable comments. Each named author has participated sufficiently in the work to
599 take public responsibility for the content. S.Y.T. and M.Y. developed the concept;
600 S.Y.T. performed the research with help from M.Y., F.C. and M.M.R; F.C., S.Y.T.
601 and H.M.H analyzed the data; S.Y.T., M.Y. and F.C. wrote the manuscript. Each of
602 the authors confirms that this manuscript has not been previously published and is not
603 currently under consideration by any other journal. Additionally, all authors have
604 approved the manuscript and agreed to its submission to Global and Planetary Change.
605 The work described in this article was partially supported by grants from the Research
606 Grants Council of the Hong Kong Special Administrative Region, China (project
607 codes: HKU 17300720, HKU 17302518, HKU 17303115), the Seed Funding
608 Programme for Basic Research of the University of Hong Kong (project codes:
609 201811159076, 201711159057, 201611159053, 202011159122), the Small
610 Equipment Grant of the University of Hong Kong, the Seed Funding of the HKU-
611 TCL Joint Research Centre for Artificial Intelligence, and the Faculty of Science RAE
612 Improvement Fund of the University of Hong Kong (to MY). HHMH is funded by the
613 Peter Buck Postdoctoral Fellowship of the National Museum of Natural History,
614 Smithsonian Institution. MMR is funded by the USGS Land Change Science

615 Research and Development Program. Any use of trade, firm, or product names is for
616 descriptive purposes only and does not imply endorsement by the U.S. Government.

617

618 **References**

- 619 Arreguin-Rodriguez, G.J., Thomas, E., D'haenens, S., Speijer, R.P. and Alegret, L., 2018.
620 Early Eocene deep-sea benthic foraminiferal faunas: Recovery from the Paleocene
621 Eocene Thermal Maximum extinction in a greenhouse world. *Plos one*, 13(2),
622 e0193167.
- 623 Bralower, T.J. et al., 2018. Evidence for Shelf Acidification During the Onset of the
624 Paleocene-Eocene Thermal Maximum. *Paleoceanography and Paleoclimatology*,
625 33(12), 1408-1426.
- 626 Bralower, T.J. and Self-Trail, J.M., 2016. Nannoplankton malformation during the Paleocene-
627 Eocene Thermal Maximum and its paleoecological and paleoceanographic
628 significance. *Paleoceanography*, 31(10), 1423-1439.
- 629 Breitbart, D. et al., 2018. Declining oxygen in the global ocean and coastal waters. *Science*,
630 359(6371), eaam7240.
- 631 Cronin, T.M., 1991. Late Neogene marine Ostracoda from Tjörnes, Iceland. *Journal of*
632 *Paleontology*, 65(5), 767-794.
- 633 Dickson, A.J., Cohen, A.S. and Coe, A.L., 2012. Seawater oxygenation during the Paleocene-
634 Eocene thermal maximum. *Geology*, 40(7), 639-642.
- 635 Foster, G.L., Hull, P., Lunt, D.J. and Zachos, J.C., 2018. Placing our current 'hyperthermal' in
636 the context of rapid climate change in our geological past. The Royal Society
637 Publishing, A376, 20170086.
- 638 Foster, W.J. et al., 2020. Resilience of marine invertebrate communities during the early
639 Cenozoic hyperthermals. *Scientific reports*, 10(1), 1-11.
- 640 Gilly, W.F., Beman, J.M., Litvin, S.Y. and Robison, B.H., 2013. Oceanographic and
641 biological effects of shoaling of the oxygen minimum zone. *Annual review of marine*
642 *science*, 5, 393-420.
- 643 Hantsoo, K.G., Kump, L.R., Haupt, B.J. and Bralower, T.J., 2018. Tracking the Paleocene-
644 Eocene thermal maximum in the North Atlantic: A shelf-to-basin analysis with a
645 regional ocean model. *Paleoceanography and Paleoclimatology*, 33(12), 1324-1338.
- 646 Huang, H.H.M. et al., 2018. Benthic biotic response to climate changes over the last 700,000
647 years in a deep marginal sea: impacts of deoxygenation and the Mid-Brunhes Event.
648 *Paleoceanography and Paleoclimatology*, 33(7), 766-777.
- 649 Huff, W., 1970. The Jackson Eocene Ostracoda of Mississippi. *Mississippi Geologic,*
650 *Economic and Topographic Survey. Bulletin*, 114, 389.
- 651 Hutchinson, D.K. et al., 2019. Arctic closure as a trigger for Atlantic overturning at the
652 Eocene-Oligocene Transition. *Nature communications*, 10(1), 1-9.
- 653 Ivany, L.C. et al., 2018. Little lasting impact of the Paleocene-Eocene Thermal Maximum on
654 shallow marine molluscan faunas. *Science advances*, 4(9), eaat5528.
- 655 John, C.M. et al., 2008. North American continental margin records of the Paleocene-Eocene
656 thermal maximum: Implications for global carbon and hydrological cycling.
657 *Paleoceanography*, 23(2), PA2217.
- 658 Kelly, D.C., Bralower, T.J., Zachos, J.C., Silva, I.P. and Thomas, E., 1996. Rapid
659 diversification of planktonic foraminifera in the tropical Pacific (ODP Site 865)
660 during the late Paleocene thermal maximum. *Geology*, 24(5), 423-426.

661 Kennett, J.P. and Stott, L., 1991. Abrupt deep-sea warming, palaeoceanographic changes and
662 benthic extinctions at the end of the Palaeocene. *Nature*, 353(6341), 225-229.

663 Kidwell, S.M. and Holland, S.M., 2002. The quality of the fossil record: implications for
664 evolutionary analyses. *Annual Review of Ecology and Systematics*, 33(1), 561-588.

665 Kiessling, W. and Simpson, C., 2011. On the potential for ocean acidification to be a general
666 cause of ancient reef crises. *Global Change Biology*, 17(1), 56-67.

667 León y León, I.A., Bralower, T.J. and Self-Trail, J.M., 2018. Ecological Changes in the
668 Nannoplankton Community Across A Shelf Transect During the Onset of the
669 Paleocene-Eocene Thermal Maximum. *Paleoceanography and Paleoclimatology*,
670 33(12), 1396-1407.

671 Lewis Steineck, P. and Thomas, E., 1996. The latest Paleocene crisis in the deep sea:
672 Ostracode succession at Maud Rise, Southern Ocean. *Geology*, 24(7), 583-586.

673 Lord, A., Whittaker, J. and King, C., 2009. Paleogene. In: J.E. WHITTAKER and M.B.
674 HART (Eds.), *Ostracods in British Stratigraphy*. The Micropalaeontological Society
675 Special Publications, pp. 374-409.

676 McInerney, F.A. and Wing, S.L., 2011. The Paleocene-Eocene Thermal Maximum: A
677 perturbation of carbon cycle, climate, and biosphere with implications for the future.
678 *Annual Review of Earth and Planetary Sciences*, 39, 489-516.

679 Morkhoven, F.v., 1962. *Post-palaeozoic Ostracoda: Their Morphology, Taxonomy and*
680 *Economic Use: Vol. I: General*. Elsevier Public. Company.

681 Morsi, A.-M.M., Speijer, R.P., Stassen, P. and Steurbaut, E., 2011. Shallow marine ostracode
682 turnover in response to environmental change during the Paleocene–Eocene thermal
683 maximum in northwest Tunisia. *Journal of African Earth Sciences*, 59(2-3), 243-268.

684 Nicolo, M.J., Dickens, G.R. and Hollis, C.J., 2010. South Pacific intermediate water oxygen
685 depletion at the onset of the Paleocene–Eocene thermal maximum as depicted in New
686 Zealand margin sections. *Paleoceanography*, 25(4).

687 Norris, R., Turner, S.K., Hull, P. and Ridgwell, A., 2013. Marine ecosystem responses to
688 Cenozoic global change. *Science*, 341(6145), 492-498.

689 Oksanen, J. et al., 2018. Package ‘vegan’ community ecology package. See [https://cran.r-](https://cran.r-project.org/web/packages/vegan/index.html)
690 [project.org/web/packages/vegan/index.html](https://cran.r-project.org/web/packages/vegan/index.html).

691 Puckett, T.M., 1994. New ostracoda species from an upper Cretaceous oyster reef, northern
692 Gulf Coastal Plain, USA. *Journal of Paleontology*, 68(6), 1321-1335.

693 Rambaut, A., Drummond, A.J., Xie, D., Baele, G. and Suchard, M.A., 2018. Posterior
694 summarization in Bayesian phylogenetics using Tracer 1.7. *Systematic biology*, 67(5),
695 901-904.

696 Robinson, M.M. and Spivey, W.E., 2019. Environmental and Geomorphological Changes on
697 the Eastern North American Continental Shelf Across the Paleocene-Eocene
698 Boundary. *Paleoceanography and Paleoclimatology*, 34(4), 715-732.

699 Scheibner, C. and Speijer, R., 2008. Late Paleocene–early Eocene Tethyan carbonate platform
700 evolution—A response to long-and short-term paleoclimatic change. *Earth-Science*
701 *Reviews*, 90(3-4), 71-102.

702 Self-Trail, J.M., 2011. Paleogene calcareous nannofossils of the South Dover Bridge core,
703 southern Maryland (USA). *Journal of Nannoplankton Research*, 32(1), 1-28.

704 Self-Trail, J.M., Powars, D.S., Watkins, D.K. and Wandless, G.A., 2012. Calcareous
705 nannofossil assemblage changes across the Paleocene–Eocene Thermal Maximum:
706 Evidence from a shelf setting. *Marine Micropaleontology*, 92, 61-80.

707 Self-Trail, J.M. et al., 2017. Shallow marine response to global climate change during the
708 Paleocene-Eocene Thermal Maximum, Salisbury Embayment, USA.
709 *Paleoceanography*, 32(7), 710-728.

710 Shin, C.P. et al., 2019. Neogene marine ostracod diversity and faunal composition in Java,
711 Indonesia: Indo-Australian Archipelago biodiversity hotspot and the Pliocene
712 diversity jump. *Journal of Crustacean Biology*, 39(3), 244-252.

- 713 Silvestro, D., Salamin, N., Antonelli, A. and Meyer, X., 2019. Improved estimation of
714 macroevolutionary rates from fossil data using a Bayesian framework. *Paleobiology*,
715 45(4), 546-570.
- 716 Silvestro, D., Schnitzler, J., Liow, L.H., Antonelli, A. and Salamin, N., 2014. Bayesian
717 estimation of speciation and extinction from incomplete fossil occurrence data.
718 *Systematic biology*, 63(3), 349-367.
- 719 Sluijs, A., Bowen, G., Brinkhuis, H., Lourens, L. and Thomas, E., 2007a. The Palaeocene-
720 Eocene Thermal Maximum super greenhouse: biotic and geochemical signatures, age
721 models and mechanisms of global change. *The Micropalaeontological Society*,
722 *Special Publications.*, 2, 323-349.
- 723 Sluijs, A. and Brinkhuis, H., 2009. A dynamic climate and ecosystem state during the
724 Paleocene-Eocene Thermal Maximum: inferences from dinoflagellate cyst
725 assemblages on the New Jersey Shelf. *Biogeosciences*, 6(8), 1755-1781.
- 726 Sluijs, A. et al., 2008. Eustatic variations during the Paleocene-Eocene greenhouse world.
727 *Paleoceanography*, 23(4), PA4216.
- 728 Sluijs, A. et al., 2007b. Environmental precursors to rapid light carbon injection at the
729 Palaeocene/Eocene boundary. *Nature*, 450(7173), 1218-1221.
- 730 Sluijs, A. et al., 2014. Warming, euxinia and sea level rise during the Paleocene–Eocene
731 Thermal Maximum on the Gulf Coastal Plain: implications for ocean oxygenation
732 and nutrient cycling. *Climate of the Past*, 10(4), 1421-1439.
- 733 Speijer, R., Scheibner, C., Stassen, P. and Morsi, A.-M.M., 2012. Response of marine
734 ecosystems to deep-time global warming: A synthesis of biotic patterns across the
735 Paleocene-Eocene thermal maximum (PETM). *Austrian Journal of Earth Sciences*,
736 105(1), 6-16.
- 737 Speijer, R.P. and Morsi, A.-M.M., 2002. Ostracode turnover and sea-level changes associated
738 with the Paleocene-Eocene thermal maximum. *Geology*, 30(1), 23-26.
- 739 Stassen, P., Speijer, R.P. and Thomas, E., 2014. Unsettled puzzle of the Marlboro clays.
740 *Proceedings of the National Academy of Sciences*, 111(12), E1066-E1067.
- 741 Stassen, P., Thomas, E. and Speijer, R.P., 2015. Paleocene–Eocene Thermal Maximum
742 environmental change in the New Jersey Coastal Plain: benthic foraminiferal biotic
743 events. *Marine Micropaleontology*, 115, 1-23.
- 744 Stramma, L. et al., 2012. Expansion of oxygen minimum zones may reduce available habitat
745 for tropical pelagic fishes. *Nature Climate Change*, 2(1), 33.
- 746 Stramma, L., Schmidtko, S., Levin, L.A. and Johnson, G.C., 2010. Ocean oxygen minima
747 expansions and their biological impacts. *Deep Sea Research Part I: Oceanographic
748 Research Papers*, 57(4), 587-595.
- 749 Thomas, E., 2007. Cenozoic mass extinctions in the deep sea: What perturbs the largest
750 habitat on Earth? *SPECIAL PAPERS-GEOLOGICAL SOCIETY OF AMERICA*,
751 424, 1.
- 752 Turner, S.K., Hull, P.M., Kump, L.R. and Ridgwell, A., 2017. A probabilistic assessment of
753 the rapidity of PETM onset. *Nature communications*, 8(1), 353.
- 754 Van Nieuwenhuise, D.S., 2007. Ostracode Biomarkers in the Paleogene of the Gulf of
755 Mexico. *Gulf Coast Association of Geological Societies Transactions*, v. 57, p. 747-
756 755.
- 757 Vellekoop, J. et al., 2018. Shelf hypoxia in response to global warming after the Cretaceous-
758 Paleogene boundary impact. *Geology*, 46(8), 683-686.
- 759 Webb, A.E., Leighton, L.R., Schellenberg, S.A., Landau, E.A. and Thomas, E., 2009. Impact
760 of the Paleocene-Eocene thermal maximum on deep-ocean microbenthic community
761 structure: Using rank-abundance curves to quantify paleoecological response.
762 *Geology*, 37(9), 783-786.
- 763 Winguth, A.M., Thomas, E. and Winguth, C., 2012. Global decline in ocean ventilation,
764 oxygenation, and productivity during the Paleocene-Eocene Thermal Maximum:
765 Implications for the benthic extinction. *Geology*, 40(3), 263-266.

766 Wood, A. and Whatley, R., 1997. The genera *Muellerina* Bassiouni, 1965 and *Thaerocythere*
767 *Hazel*, 1967 from the Neogene of Northwest Europe. *Journal of Micropalaeontology*,
768 16(1), 1-18.

769 Yamaguchi, T. and Norris, R.D., 2012. Deep-sea ostracode turnovers through the Paleocene–
770 Eocene thermal maximum in DSDP Site 401, Bay of Biscay, North Atlantic. *Marine*
771 *Micropaleontology*, 86, 32-44.

772 Yamaguchi, T. and Norris, R.D., 2015. No place to retreat: Heavy extinction and delayed
773 recovery on a Pacific guyot during the Paleocene–Eocene Thermal Maximum.
774 *Geology*, 43(5), 443-446.

775 Yamaguchi, T., Norris, R.D. and Bornemann, A., 2012. Dwarfing of ostracodes during the
776 Paleocene–Eocene Thermal Maximum at DSDP Site 401 (Bay of Biscay, North
777 Atlantic) and its implication for changes in organic carbon cycle in deep-sea benthic
778 ecosystem. *Palaeogeography, Palaeoclimatology, Palaeoecology*, 346, 130-144.

779 Yamaguchi, T., Norris, R.D. and Dockery III, D.T., 2014. Shallow-marine ostracode turnover
780 during the Eocene–Oligocene transition in Mississippi, the Gulf Coast Plain, USA.
781 *Marine Micropaleontology*, 106, 10-21.

782 Yasuhara, M. and Cronin, T.M., 2008. Climatic influences on deep-sea ostracode (Crustacea)
783 diversity for the last three million years. *Ecology*, 89(sp11), S53-S65.

784 Yasuhara, M., Cronin, T.M., deMenocal, P.B., Okahashi, H. and Linsley, B.K., 2008. Abrupt
785 climate change and collapse of deep-sea ecosystems. *Proceedings of the National*
786 *Academy of Sciences*, 105(5), 1556-1560.

787 Yasuhara, M., Doi, H., Wei, C.-L., Danovaro, R. and Myhre, S.E., 2016. Biodiversity–
788 ecosystem functioning relationships in long-term time series and palaeoecological
789 records: deep sea as a test bed. *Phil. Trans. R. Soc. B*, 371(1694), 20150282.

790 Yasuhara, M. et al., 2019. Eocene shallow-marine ostracods from Madagascar: southern end
791 of the Tethys? *Journal of Systematic Palaeontology*, 17(9), 705-757.

792 Yasuhara, M., Hunt, G., Okahashi, H. and Brandao, S.N., 2015. Taxonomy of deep-sea
793 trachyleberidid, thaerocytherid, and hemicytherid genera (Ostracoda). *Smithsonian*
794 *Contributions to Paleobiology*.

795 Yasuhara, M. et al., 2017a. Cenozoic dynamics of shallow-marine biodiversity in the Western
796 Pacific. *Journal of Biogeography*, 44(3), 567-578.

797 Yasuhara, M., Okahashi, H., Cronin, T.M., Rasmussen, T.L. and Hunt, G., 2014. Response of
798 deep-sea biodiversity to abrupt deglacial and Holocene climate changes in the North
799 Atlantic Ocean. *Global Ecology and Biogeography*, 23(9), 957-967.

800 Yasuhara, M., Tittensor, D.P., Hillebrand, H. and Worm, B., 2017b. Combining marine
801 macroecology and palaeoecology in understanding biodiversity: microfossils as a
802 model. *Biological Reviews*, 92(1), 199-215.

803 Zachos, J.C., Dickens, G.R. and Zeebe, R.E., 2008. An early Cenozoic perspective on
804 greenhouse warming and carbon-cycle dynamics. *Nature*, 451(7176), 279.

805 Zachos, J.C. et al., 2006. Extreme warming of mid-latitude coastal ocean during the
806 Paleocene-Eocene Thermal Maximum: Inferences from TEX86 and isotope data.
807 *Geology*, 34(9), 737-740.

808 Zhang, L., Hay, W.W., Wang, C. and Gu, X., 2019. The evolution of latitudinal temperature
809 gradients from the latest Cretaceous through the Present. *Earth-Science Reviews*, 189,
810 147-158.

811 Zizka, A. et al., 2019. CoordinateCleaner: Standardized cleaning of occurrence records from
812 biological collection databases. *Methods in Ecology and Evolution*, 10(5), 744-751.

813

814